energies

MDPI

Article

Numerical Study of Heat Transfer Intensification in a Circular Tube Using a Thin, Radiation-Absorbing Insert. Part 2: Thermal Performance

Piotr Bogusław Jasiński

Institute of Turbomachinery, Lodz University of Technology, 90-924 Lodz, Poland; piotr.jasinski@p.lodz.pl; Tel.: +48-42-631-23-49

Abstract: This article is the second part of the work under the same title, which is based on the results of the research presented in the previous article: "Numerical study of heat transfer intensification in a circular tube using a thin, radiation-absorbing insert. Part 1: Thermo-hydraulic characteristics". Part 1 presents an analysis of pressure drops and heat transfer intensification in a round tube with an insert, using the phenomenon of radiation absorption. In this paper, an analysis of the tested insert's thermal performance (PEC) is presented, taking into account the criterion of equal pumping power. The tests were carried out for the range of Re = 5000–100,000 numbers, for various insert diameters (from 20% to 90% of the pipe diameter) and a constant temperature difference between the wall and the gas $\Delta T = 100$ °C. The highest Nu numbers were observed for inserts with dimensionless diameters of 0.3 and 0.4, while the highest flow resistance was observed for inserts with diameters of 0.6 and 0.7 of the channel diameter. The thermal efficiency was calculated in two ways, as was the associated Nu number. These results significantly differed from each other: the maximum PEC values for method (I) reached 2, and for method (II) to 8. The common feature for both calculation methods was the fact that the maximum values of the Nu number and the thermal efficiency were observed for small Re numbers; however, as the Re number increases, PEC and Nu number decrease strongly.

Keywords: heat transfer enhancement; radiation insert; numerical simulations; performance evaluation criteria; thermal efficiency

check for updates

Citation: Jasiński, P.B. Numerical Study of Heat Transfer Intensification in a Circular Tube Using a Thin, Radiation-Absorbing Insert. Part 2: Thermal Performance. *Energies* **2021**, *14*, 4533. https://doi.org/10.3390/14154533

Academic Editor: Pouyan Talebizadeh Sardari

Received: 15 June 2021
Accepted: 21 July 2021
Published: 27 July 2021

1. Introduction

The challenge for heat exchanger designers is to achieve high heat transfer intensification, which is always associated with increased flow resistance in the channels. This phenomenon, increases the amount of energy consumed to pump the fluid, mainly due to the turbulisation of the flow. One of the most commonly used parameters to evaluate thermal channels is the thermal performance factor (TPF) or otherwise known as performance evaluation criteria (PEC) [1–3]. It compares the duct under test to a smooth round pipe, with the same thermal conditions and the same pumping power. If the PEC is greater than unity, then such a channel is considered to be more thermally efficient than a smooth pipe (the goal is to achieve the highest possible values), and if it is less than unity, the thermal efficiency of such a channel after modification is worse than a smooth pipe.

Many authors apply this method of evaluation in examining heat channels with turbulising inserts, porous material, or with internally ribbed walls [4–7]. These heat transfer intensification mechanisms rely on the fluid flow disturbance in the channel's entire cross-section (inserts) or only at the wall (micro-ribs). It can be said that all methods of convective heat transfer intensification are aimed at reducing the thickness of the laminar boundary layer or even breaking it locally, which, as is known, is the main resistance in convective heat transport.

The article presents the results of testing channels with an insert that does not turbulise the flow like most elements of this type but uses an additional heat transfer mechanism, i.e., thermal radiation. Due to the necessary radiation transmittance of the working fluid, this method can only be used for transparent gases.

The insert presented in this article is made in the form of a thin, smooth pipe and placed parallel and concentrically to the flow channel walls (Figure 1). In addition to the standard convective heat transport method between the pipe wall and the fluid, the phenomenon of thermal radiation between the wall, and the insert is also used as a heat transfer intensification mechanism. During the fully developed fluid flow, the insert placed in the centre of the tube does not cause fluid mixing between the boundary layer and the turbulent core. The temperature of the insert differs from that of the wall and depends on its diameter and flow conditions. Due to the temperature difference, heat is transferred by radiation between the wall and the insert surface. Assuming that the working gas is completely transparent and does not absorb radiation, the total radiant heat flux is transferred to the insert, which consequently becomes an additional heat transfer surface, giving up heat energy to the fluid on both sides by convection.

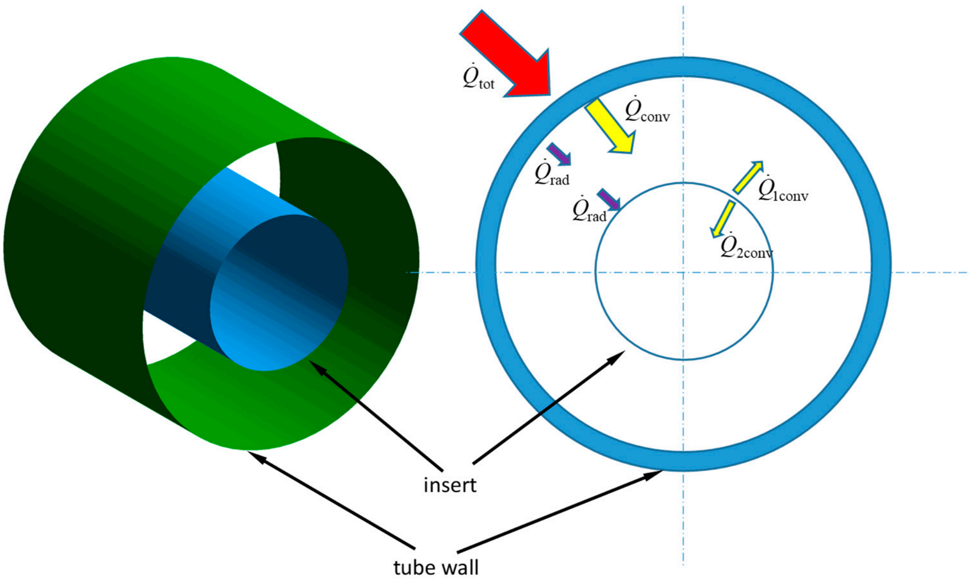

Figure 1. A fragment of a pipe with an insert and a diagram of heat fluxes.

Alijani and Hamidi, in their works [8,9], presented research of inserts, in which the mode of operation was most similar to that presented in this article. They experimentally studied inserts in the form of a solid rod inserted into a pipe [8], while in the second case [9], the insert had a honeycomb cross-section. Both inserts intensified the heat transfer using the effect of thermal radiation. The authors investigated rods with constant dimensions and at different temperatures of the pipe wall. The highest thermal efficiency values (up to 4–5) were obtained for the honeycomb insert, for the highest wall temperatures about 400 °C, and the lowest Reynolds numbers 5000–7000. In turn, Zhang et al. [10] investigated a fully developed channel flow with a porous core in the centre. The numerical analysis confirmed the effectiveness of the porous core in increasing the intensity of heat transfer. The proposed system has been particularly effective for a gaseous medium with low emittance and low fluid velocities. It was also observed that increasing the porous core diameter increases the heat transfer intensity, but the flow resistance also increases.

As previously mentioned, this article is a continuation of the previous work under the same title [11], and the presented results are based on the data from that paper. Numerical simulations were performed using the ANSYS-CFX computer code. It was chosen as a computational tool both because of its flexibility and reliability and also because of the extensive experience acquired over many years by our research groups, as applied to various thermal and flow problems [12–14].

This work's originality is based on the use of an additional heat transport mechanism, which is radiation from the pipe wall to the absorption insert. The presented results were obtained for a relatively small temperature difference ΔT = 100 °C, as for radiation processes. The concept of this type of insert may be of great importance, especially for high-temperature combustion and heat recovery processes, where thermal radiation is the dominant method of heat transfer.

In general, the main purpose of this work is to investigate the relationship between the geometric dimension of the insert, i.e., its diameter, in relation to the heat efficiency of the pipe. The heat transfer enhancement with respect to the pipe without insert, considering the criterion of the same pumping power shows the PEC coefficient.

2. Geometric Model of the Insert

According to the scheme in Figure 1, the total heat flux $\dot{Q}_{\mathrm{tot}}$ delivered to the channel's outer wall is partly transferred by convection $\dot{Q}_{\mathrm{conv}}$ to the fluid, and the rest of this flux $\dot{Q}_{\mathrm{rad}}$ is transferred to the insert by radiation. Thus, the balance equation of such a system has this form:

$$\dot{Q}_{\mathrm{tot}} = \dot{Q}_{\mathrm{conv}} + \dot{Q}_{\mathrm{rad}} = \dot{Q}_{\mathrm{conv}} + \left(\dot{Q}_{\mathrm{1conv}} + \dot{Q}_{\mathrm{2conv}}\right) \tag{1}$$

During the fully developed channel flow, a temperature difference exists between the wall surface and the insert, causing the radiant heat flux $\dot{Q}_{\mathrm{rad}}$ to be transferred to the insert. Due to the fact that the insert does not cause turbulising and mixing of the fluid, its temperature is a function of its radius. The radiative heat flux is absorbed by the insert, causing its temperature to rise slightly above the flowing gas's boundary layer's local temperature. Simultaneously, the insert is washed by the working gas (which flows both outside and inside the insert) and gives off the heat on both sides in a convective manner (heat fluxes $\dot{Q}_{\mathrm{1conv}}$ and $\dot{Q}_{\mathrm{2conv}}$, Figure 1). Such an insert can thus actually be treated as an additional heat transfer surface inside the duct.

The thickness of such an insert should be as small as possible and should be made of a material that conducts heat well. You can then ignore the wall thickness and assume that its temperature is the same on both sides. In order to obtain the highest possible radiative heat flux, the emissivity of both radiating surfaces: the pipe wall and the outer insert, should also be as high as possible.

The practical application of such an insert may be particularly appropriate in high-temperature heat exchangers. Due to a significant temperature difference, the radiation fraction in heat transfer is significant compared to convection, e.g., heat recovery from exhaust gases in gas boilers, cars, etc. Nevertheless, the use of such an insert even at a small temperature difference of 100 °C, as presented in the paper, significantly increases the heat transfer efficiency in the heat exchanger channel.

3. Boundary Conditions of Simulation and Numerical Model

Numerical simulations were performed for eight insert diameters d_{i}. In all cases, the same temperature difference ΔT = 100 °C was maintained between the wall and the average gas temperature in the pipe's entire volume. The heat transfer boundary condition of the 1st kind was applied on the channel's outer wall, i.e., a constant wall temperature equal to 100 °C. The list of used boundary conditions are introduced in Table 1.

For gas, on the other hand, the mean volume temperature was kept constant at 0 °C. The working gas was the air with physical properties dependent on temperature and complete transparency for radiation. In Table 2, the coefficients of polynomial equations for thermal conductivity and dynamic viscosity of the air were shown.

Table 1. Boundary conditions and the parameters values.

Boundary Condition	Description	Parameter	Value/Type
Fluid Domain	Air	Mean Temperature	273 K
		Reference Pressure	1 atm
		Turbulence Model	SST k-ω
Subdomain	Subdomain was set in domain of air. The pressure gradient determined according to the flow direction.	Pressure gradient	0.025–8 Pa/m
		Volumetric heat flux	$-Q_{vol} = \frac{Q_{tot} \cdot A_2}{V_{air}}$ W
Wall	Boundary condition set on the wall of pipe in the form of constant Temperature	Temperature	373 K
Translational Periodicity	Translational Periodicity set on the inlet and outlet areas of Fluid Domain.	-	-
Rotational Symmetry	Rotational Symmetry set on the both sides of Fluid Domain.	-	-

Table 2. Coefficients of polynomial equation $k(T)$, $\mu(T)$ = $a_0 + a_1 \times T + a_2 \times T^2 + a_3 \times T^3$ for the air temperature range 173–373 K.

		a_0	a_1	a_2	a_3
thermal conductivity	$k(T)$	-1.8650×10^{-3}	1.1018×10^{-4}	-5.6729×10^{-8}	1.6728×10^{-11}
dynamic viscosity	$\mu(T)$	2.0251×10^{-6}	6.3507×10^{-8}	-3.0959×10^{-11}	7.8708×10^{-15}

In order to simplify the notation and the possibility of reference to other geometrical dimensions, the insert diameters d_i are presented in a dimensionless form $D = d_p/d_i$ (Figure 2), in relation to the pipe's diameter d_p = 200 mm. The values of d_i and D, along with their exact dimensions, are given in Table 3.

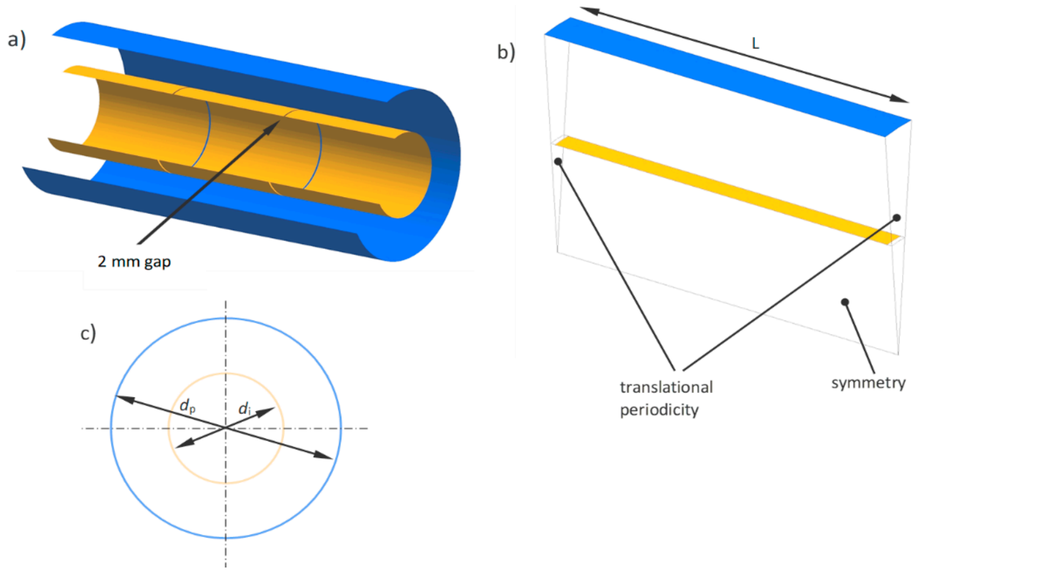

Figure 2. Repeatable insert segment: (**a**) 3D view of a pipe fragment with an insert; (**b**) computational domain; (**c**) channel cross-section diagram.

Table 3. Dimensions of the tested insert and the corresponding dimensionless diameters.

d_i [mm]	40	60	80	100	120	140	160	180
D [-]	0.2	0.3	0.4	0.5	0.6	0.7	0.8	0.9

Due to the axial nature of the flow and the lack of a rotational velocity component, it was assumed that each tested insert could be considered as a two-dimensional case. Therefore, in the simulations, as the computational domain, the geometry in the shape of a longitudinal section of a cylinder with an aperture angle of 10° and length L = 152 mm was used (Figure 2b). An axial symmetry— on the pipe section's side faces as the domain's side boundary conditions—was set.

The appropriate method of carrying out numerical simulations allowed us to obtain a fully developed flow in this relatively short domain. In order to achieve such an effect, a translational periodicity (as boundary conditions) at the inlet and outlet of the domain was set, and the fluid flow by a pressure gradient was forced. Thus, the computational domain has been reduced to a repetitive, periodic, and axisymmetric geometry representative of the entire channel. By reducing the domain size and the number of computational mesh nodes (up to 2D), it was possible to significantly shorten the computation time while maintaining the high mesh quality. Such a research method has also been presented in [15–17], while other, less important details, generally related to such a method of numerical modelling, are presented in [18–20]. In order to ensure the same static pressure on both sides of the insert, small gaps in the continuity of the insert with a 2 mm length were made (Figure 2a), representing about 1.5% of the total length of the insert. These gaps, due to their minimal size, did not disturb the flow.

For the mentioned boundary condition applied to the pipe wall (temperature of 100°), the heat flux supplied to the gas changes for each insert geometry and flow rate. In order to obtain a periodic thermal layer and preserve the energy balance in the domain, the heat flux supplied to the domain was compensated by applying a negative volumetric energy source $\dot{Q}_{\text{vol}}$, i.e., subtracting from the entire flow domain the same amount of heat energy that was supplied by the wall surface (Figure 3).

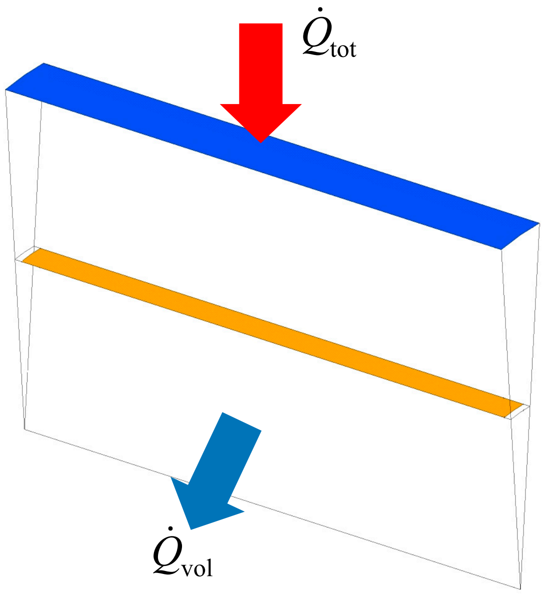

Figure 3. Scheme of the computational domain with supplied and withdrawn heat flux.

3.1. Governing Equations

Numerical calculations of the frictional resistance and the heat transfer were performed using the ANSYS-CFX code. During calculations are solved the basic equations of conservation of mass (2), momentum (3) and energy (4), which have the form [21]:

$$\frac{\partial \rho}{\partial t} + \nabla \cdot (\rho \overline{U}) = 0 \tag{2}$$

$$\frac{\partial(\rho\overline{U})}{\partial t} + \nabla \cdot (\rho\overline{U} \times \overline{U}) = -\nabla p + \nabla \cdot \mu_e(\nabla\overline{U} + (\nabla\overline{U})^T - \frac{2}{3}\delta\nabla \cdot \overline{U}) + (\rho - \rho_{ref})g \quad (3)$$

$$\frac{\partial(i_{tot}\rho)}{\partial t} = \frac{\partial\rho}{\partial t} + \nabla \cdot (\rho\overline{U}i_{tot}) = \nabla \cdot (k\nabla T) + \nabla \cdot (\overline{U}\tau_w) + S_E \quad (4)$$

where the term $\nabla \cdot (\overline{U}\tau_w)$ represents the work of viscous forces, S_E is a term of an energy sources and the total enthalpy i_{tot} is expressed as:$i + \frac{1}{2}\overline{U}^{\,2}$. For the turbulence model used, the governing equations are presented in detail in [17].

3.2. Turbulence Model

The turbulence model SST k-ω (Shear Stres Transport) in all numerical simulations was used due to the assumed turbulent fluid flow. It is one of the most frequently used models in CFD applications due to the much better mapping of flow-thermal phenomena in calculations than the standard k-ε model [17,21]. The SST model's main advantage is the ability to take into account a viscous boundary sublayer by applying the k-ω model near the wall and using the standard k-ε model in the turbulent core region. A special function (so-called blending function) implemented in the SST model is responsible for selecting an appropriate calculation model.

3.3. Radiation Model

Several radiation models are available in the ANYS-CFX calculation program, such as Rosseland, P1, Discrete Transfer and Monte Carlo. In a situation where the thermal radiation energy is transferred between two surfaces, and the medium is transparent to radiation with wavelengths in which most of the heat transfer takes place, the Monte Carlo model is the only one that applies—and this model was used in the simulations [21]. The remaining details of the radiation model validation are described in Part 1 of this article [11].

3.4. Grid Independence

The actual simulations were preceded by performing verification calculations for several geometries at different mesh densities. Table 4 gives an example of the grid under test for one of the insert diameter $D = 0.4$ and Re = 18650. It was observed that the deviation between the grid elements of 25,440 and 49,820 is only 0.9% for friction factor and 0.22% for Nu number. Thus, for further calculations, a structural and hexagonal mesh (Figure 4) with 25,440 elements was chosen and such quality, at which its further densification gives results differing by less than 1.5%. Due to the fact that for such geometries, the velocity field structure is not very complicated and similar to the flow in a smooth pipe; therefore, the computational grid is also simple. Only in the near-wall laminar sublayer areas, i.e., at the channel wall and on both sides of the insert, the mesh was additionally densified to obtain the appropriate y^+ value, which for the used SST k-ω turbulence model should not exceed 2 [2,16,17,21,22].

Table 4. Grid independent test for Re = 18650 and insert diameter $D = 0.4$.

No. of Elements	f	dev. %	Nu	dev. %
6140	0.0461	-	73.23	-
11,960	0.0508	9.38	78.05	6.18
18,230	0.0543	6.32	80.13	2.60
25,440	0.0551	1.45	80.62	0.61
49,820	0.0556	0.9	80.80	0.22

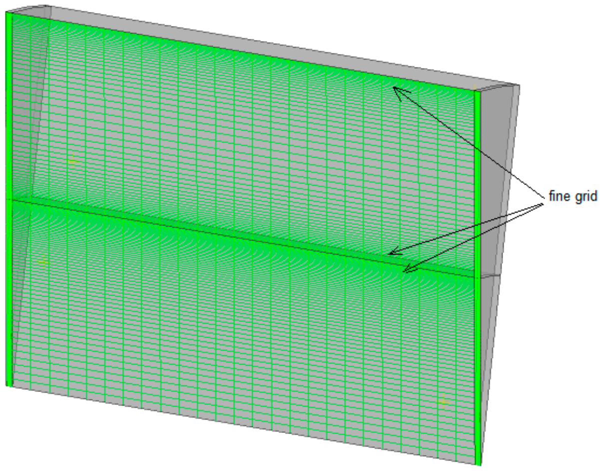

Figure 4. Computational mesh with densification areas at the walls.

Nevertheless, validation for numerical results was done, but for slightly different flow channel shapes and presented in papers [16,19,23].

4. Data Processing

To calculate the Nu number from numerical simulations, the following dependency was used:

$$Nu = \frac{\dot{Q}_{\mathrm{tot}} \cdot d_{\mathrm{p}}}{k \cdot (T_{\mathrm{w}} - T_{\mathrm{b}}) \cdot A_2} \quad (5)$$

while the Nu number for a smooth pipe without an insert was calculated from the Dittus-Boelter correlation:

$$Nu_{\mathrm{s}} = 0.023 \cdot Re^{0.8} \cdot Pr^{0.4} \quad (6)$$

The Re number is a function of the average velocity u and the pipe diameter d_{p}:

$$\mathrm{Re} = \frac{u \cdot d_{\mathrm{p}}}{\nu} \quad (7)$$

For the numerical calculations, the friction factor from the Darcy–Weisbach equation was calculated:

$$f = \frac{2 \cdot d_{\mathrm{p}}}{\rho \cdot u^2} \cdot \frac{dp}{dx} \quad (8)$$

The quantity forcing the fluid flow was the pressure gradient $\mathrm{d}p/\mathrm{d}x$, while the average velocity in the pipe u resulted from numerical calculations.

To calculate the friction factor for a smooth pipe, the Blassius formula was used:

$$f_{\mathrm{s}} = 0.3164 \cdot Re^{-0.25} \quad (9)$$

According to the same pumping power criterion, the PEC coefficient was calculated from the relationship:

$$PEC = \frac{Nu/Nu_{\mathrm{s}}}{(f/f_{\mathrm{s}})^{\frac{1}{3}}} \quad (10)$$

Both the Nu number and the friction factor f were calculated on the basis of results obtained from the numerical simulation, using Equations (2) and (5) respectively. In Equation (2), the constant values were: wall temperature T_{w}, pipe diameter d_{p} and the related wall area A_2, while the resulting values were: total heat flux on the wall Q_{tot} and bulk temperature T_{b}. Whereby, T_{b} was calculated as the volume average, and Q_{tot} as the area average. Similarly, when calculating the friction factor from Equation (5), the constant values were pipe diameter d_{p} and pressure gradient dp/dx, which was the parameter forcing the fluid flow. The resulting value from the calculations was the mean velocity u in the channel cross-section.

5. Results and Discussion

This section may be divided by subheadings. It should provide a concise and precise description

5.1. Heat Fluxes Balance

The insert's operation, consisting of intensifying the pipe's heat transfer, is possible due to the wall's temperature difference and the insert. As previously mentioned, the insert's temperature depends on its diameter and the gas flow velocity and is a key parameter on which the radiation heat flux absorbed by the insert depends. Figure 5 shows the inserts' temperature as a function of the Re number, together with the temperature difference ΔT marked schematically.

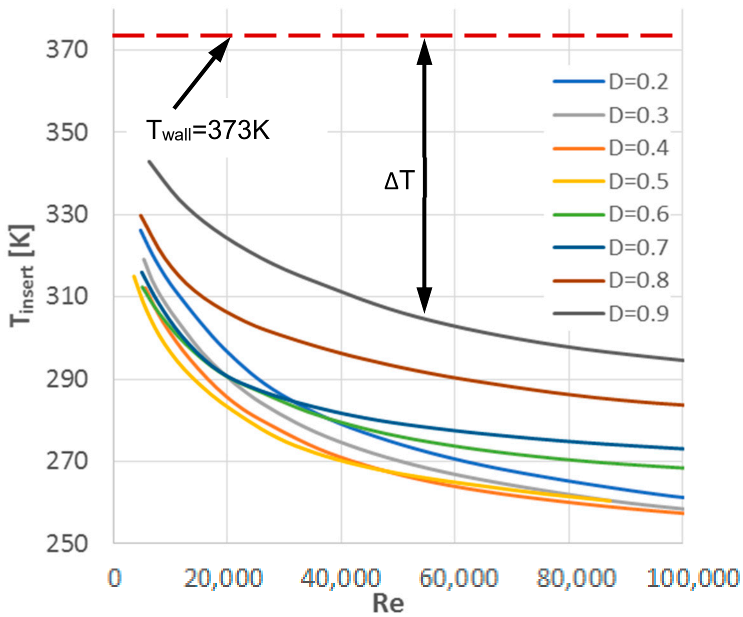

Figure 5. The tested inserts temperatures as a function of the Re number.

The highest insert temperatures occur for small Re numbers and decrease with increasing the Re numbers. As can be seen in Figure 5, in the tested Re number range, the insert temperature can change even by about 40–50 °C. As it results from the Stefan–Boltzmann law for grey bodies, the net radiative heat flux exchanged between the surfaces is a highly nonlinear function and mainly depends on the difference of the fourth powers of the surface temperatures (11).

$$Q_{rad} = \frac{\sigma \cdot A_1 \cdot \left({T_1}^4 - {T_2}^4\right)}{\frac{1}{\varepsilon_1} + \frac{A_1}{A_2} \cdot \left(\frac{1}{\varepsilon_2} - 1\right)} = \varepsilon_{12} \cdot \sigma \cdot A_1 \cdot \left({T_1}^4 - {T_2}^4\right) \tag{11}$$

The term of Equation (11), which takes into account the ratio of the heat transfer surfaces (pipe and insert) and their emissivity, is called the interchange factor (12).

$$\varepsilon_{12} = \frac{1}{\frac{1}{\varepsilon_1} + \frac{A_1}{A_2} \cdot \left(\frac{1}{\varepsilon_2} - 1\right)} \tag{12}$$

The greater the temperature difference between the surfaces, the greater radiative heat flux transferred between them. In the case of the tested inserts, the amount of this flux is also influenced by the heat transfer area ratio, which is different for each tested geometry due to the insert's changing diameter.

The total heat flux transferred to the fluid from the pipe wall consists of the radiation and convection parts (13), according to the diagram shown in Figure 1.

$$\dot{Q}_{tot} = \dot{Q}_{conv} + \dot{Q}_{rad} \tag{13}$$

In Figure 6, the fractions of the radiative (a) and convection flux (b) in relation to the total heat flux on the pipe wall are shown. As can be seen from the graphs, the greatest amount of heat energy is transferred by radiation to the inserts with the largest diameters, while the highest convective heat fluxes are observed for the smallest inserts. For all studied geometries, the tendency is that with the Re number increase, the fraction of the radiative heat flux decreases and the convective flux increases.

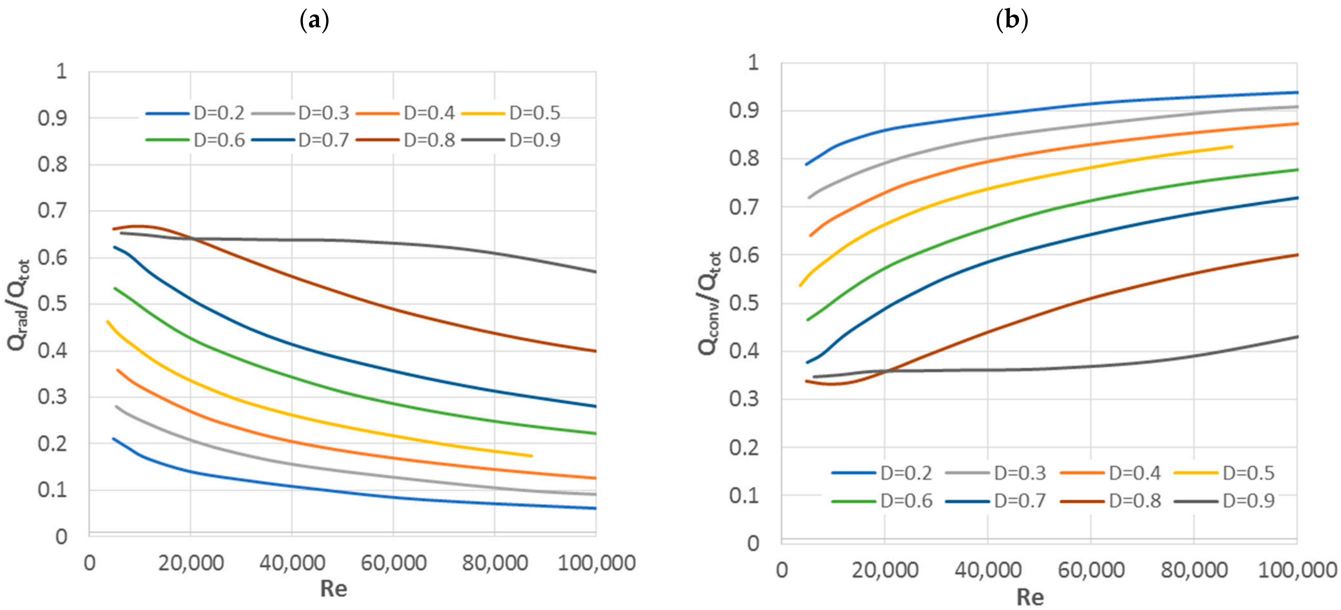

Figure 6. Fractions of radiative (**a**) and convective (**b**) heat fluxes in the total heat flux at the pipe wall.

The insert fully absorbs the radiative heat flux radiated by the pipe wall. As a result of absorbing certain thermal energy, the insert changes its temperature above the local gas temperature and gives off the heat on both sides in a convective manner (14), Figure 1.

$$\dot{Q}_{rad} = \dot{Q}_{1conv} + \dot{Q}_{2conv} \tag{14}$$

The heat flux $\dot{Q}_{1conv}$ is assumed by the flowing fluid outside the insert while $\dot{Q}_{2conv}$ is transferred to the fluid flowing inside the insert. Figure 7 shows the fractions of these heat fluxes in relation to the radiation flux absorbed by the insert. The presented graphs show the negative fractions and fractions greater than 1. Negative fractions, Figure 7a mean that above a certain Re number, the convective heat flux changes direction and the insert are additionally heated by gas from the outside. For the internal convective flux (associated with the external flux), the fractions greater than 1 were observed, Figure 7b. This means that thermal energy is transferred by convection from the insert's outer space to its inner space. If such a phenomenon occurs, it can be said that the insert only works one-sidedly, which significantly reduces the intensification of heat transfer. In Figure 7, it can be seen that the two inserts with dimensionless diameters D = 0.8 and D = 0.9, almost in the entire range of Re numbers, work this way. However, in the remaining inserts, such a phenomenon occurs only for larger Re numbers.

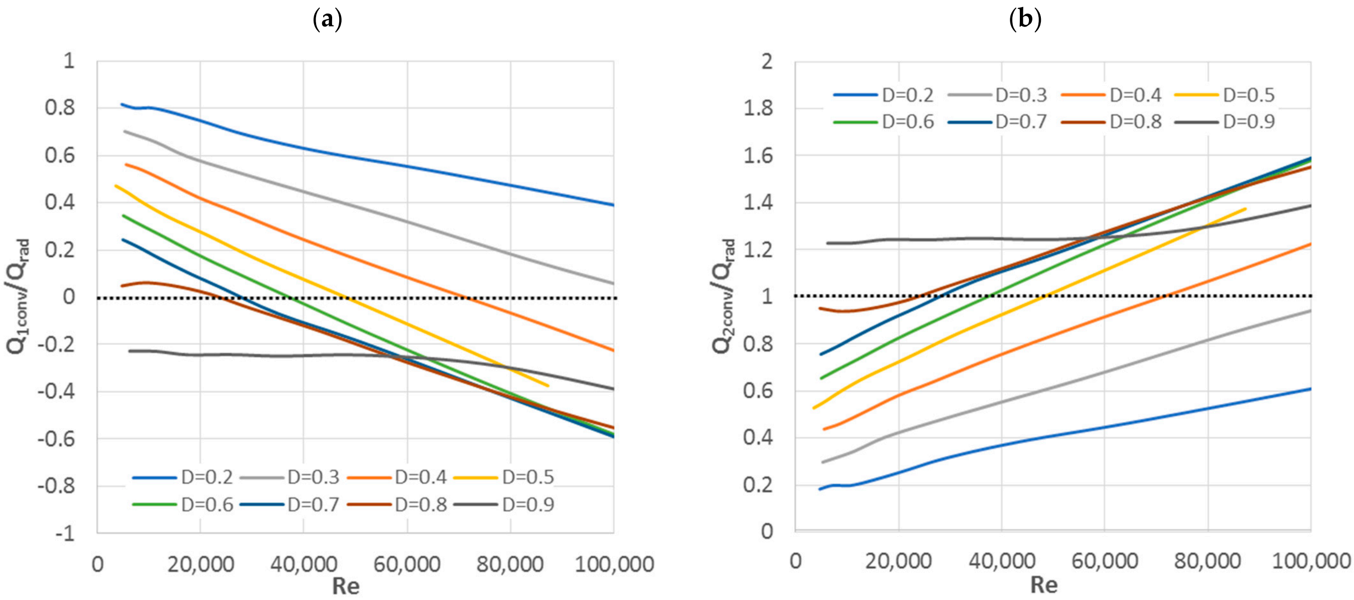

Figure 7. Fractions of convective heat fluxes on the insert surface in relation to the heat flux delivered to the insert by radiation Q_{rad}. (**a**) Q_{1conv}—heat flux on the outer surface of the insert, (**b**) Q_{2conv}—heat flux on the inner surface of the insert.

Figure 8 shows the pipe cross-section temperature profiles for a selected insert with a diameter of D = 0.4 and a few Re numbers. These examples show how the insert temperature and the gas temperature in the pipe change as a function of the radius, depending on the Re number. As can be seen, up to a Re number of about 40,000, on both sides of the insert, the gas temperature is lower than that of the insert, which means that it gives two-sided heat to the fluid by convection. For the highest number of Re = 86,500, the gas temperature in the annular section is higher than the inserts, so in this case, the insert is convectionally heated by the gas. This phenomenon causes the insert to return heat to the gas only through its inner surface, significantly reducing its thermal efficiency.

5.2. PEC Coefficient

In Part 1 of this article [11], the method of calculating the friction factor, Nu number and the analysis of the obtained results are presented. The thermal efficiency (PEC) determines how much the heat transfer's intensity will increase after the insertion in relation to the smooth pipe while maintaining the same pumping power criterion. This coefficient is calculated using the Formula (10). PEC values above unity are favourable and indicate the predominant effect of heat transfer intensification than flow resistance, while values below unity indicate greater flow resistance in relation to the benefit obtained from intensifying heat transfer of the tested geometry. Therefore, to calculate PEC, it is necessary to know the ratio f/f_s and Nu/Nu_s as a function of the Re number.

In Figure 9a the ratio f/f_s as a function of the Re number is presented, showing how many times the friction factor has increased for a given insert diameter in relation to the pipe without the insert. As you can see, for all geometries, the greatest increase is for small Re numbers, while from Re about 20,000, the characteristics are more or less horizontal, which means that the trend is similar to that for a smooth pipe. In turn, in Figure 9b, which shows the ratio f/f_s as a function of the dimensionless insert diameter D, one can observe this diameter's influence on a few selected Re numbers' friction factor. There is a clear maximum for all characteristics, ranging from 0.5–0.7D, which means the highest flow resistances for these insert diameters.

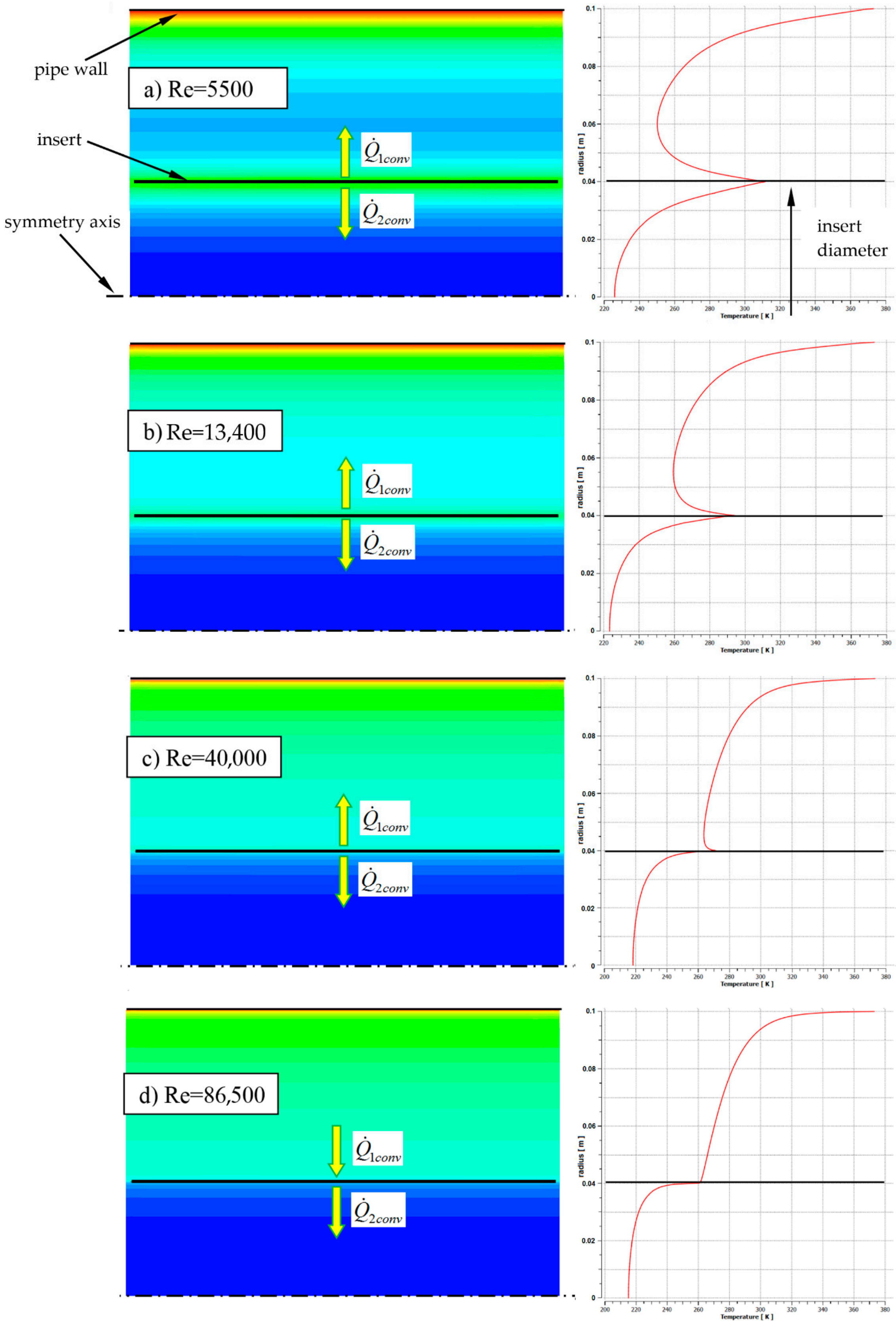

Figure 8. Temperature fields and profiles in the pipe cross-section for an exemplary insert with a diameter of D = 0.4 and several Re numbers.

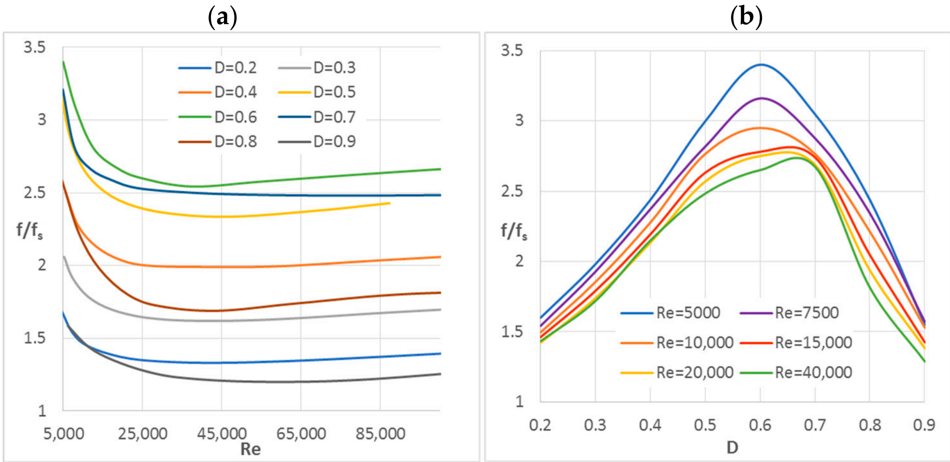

Figure 9. (**a**) the ratio $f/f_s(Re)$ for dimensionless diameters D; (**b**) the ratio $f/f_s(D)$ for several Re numbers.

The Nu number, calculated according to (1), characterises the heat transfer intensity on the channel flow wall, in this case, a round pipe. The insert divides the channel cross-section into two parts in the performed tests: annular (outside the insert) and tubular (inside the insert). This raises the question of calculating the temperature T_b, which can be related to (a) the entire volume of the pipe, (b) only the volume of the annular part that actually contacts with the channel wall. Both approaches have their justification.

ad. (a) T_b *calculated as the average volumetric temperature of the whole channel*. This method of calculation is most often used by most researchers, both for empty channels and those equipped with inserts or other turbulators, e.g., [22–32]. The heat flux is transferred to the fluid in contact with the channel wall, and its average temperature is a result of the heat transfer conditions and the medium's velocity on both sides of the insert. A certain disadvantage of this approach with the insert under consideration is the lack of fluids mixing from the annular and tubular spaces, as is the case in reality. For this reason, there are different velocity and temperature fields in these areas, and the temperature gradient in the boundary layer of the channel is completely different from what it would be with a classic insert.

ad. (b) T_b *calculated as the volumetric average temperature from the annular part only*. This approach is justified because the heat flux is directly transferred to the fluid in contact with the channel wall. Of course, its average temperature is also influenced by the amount of heat supplied to the insert by radiation and returned by the insert to the fluid by convection in the annular and tubular portions.

The author suggests that both ways of computing the Nu number can be considered, despite the fact that they give different results. Part 1 of this article [11] presents and analyses the Nu (Re) number characteristics calculated for the methods (a) and (b). A specific feature is that Nu numbers are smaller than for a smooth tube—mainly for the largest insert diameters and large Re numbers. With standard turbulising inserts, such a phenomenon should not occur because any insert placed in the pipe disturbs the flow, intensifying the convective heat flux simultaneously increasing the flow resistance.

In the case of the tested inserts, the appearance of Nu numbers lower than the reference level, which is the smooth pipe, can be explained by the creation of additional space between the pipe wall and the insert (annular section). The larger the insert diameter, the smaller the annular cross-section becomes, and at the same time, the average gas temperature in it increases, and its velocity decreases. This makes this space-gap a kind of insulation layer between the pipe wall and the main stream of gas flowing through it. With small diameters, the insert is washed on both sides by the fluid more or less evenly. On the other hand, with large diameters, the flowing gas's mass flow and its velocity are much smaller in the annular section than inside the insert. Therefore, the convective heat transfer is significantly reduced there, and the resistance from heat conduction of the gas inside the gap increases.

Figure 10a,b show the ratio of the Nu number of the tested inserts to the Nu number for a smooth pipe for the two above-mentioned calculation methods. Taking into account the average temperature Tb of the entire pipe volume (case a), it can be seen that for inserts with diameters D = 0.9, 0.8, 0.7 and 0.6, the values of the Nu/Nus characteristics are lower than unity. On the other hand, taking the average temperature Tb for the calculations only from the annular cross-section (case b), the function lines are arranged in an "ideal" order, i.e., as the insert's diameter increases, the heat transfer intensity also increases.

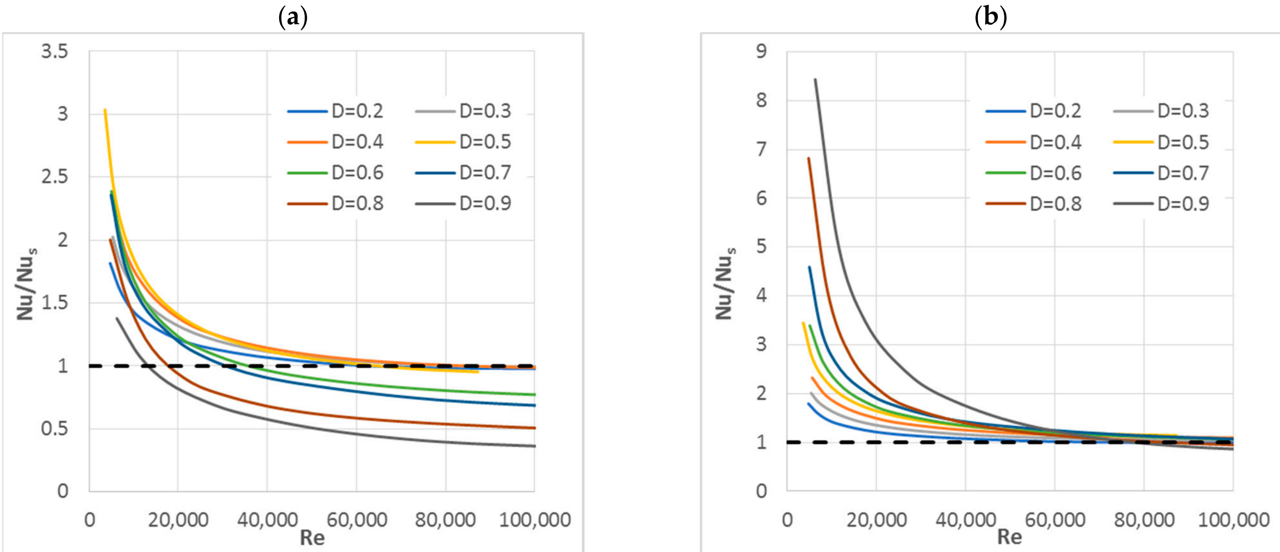

Figure 10. The ratio of the Nu number obtained from the simulation to the Nu number for a smooth pipe $Nu/Nu_s(Re)$, calculated for the mean volumetric temperature: (**a**) from the entire pipe, (**b**) from the annular section.

The thermal efficiency of the studied geometries, based on the two methods of calculating the Nu number, is shown in Figure 11. PEC coefficient calculated by method (a) reaches values much lower than that calculated by method (b). As you can see, the max PEC value calculated by method (a) is approx. 2 for the insert diameter D = 0.6, while the value calculated by method (b) reaches a value over 8 for D = 0.9.

When comparing Figures 10 and 11, a fairly large similarity can be seen in the position of the function lines. The PEC coefficients calculated in two ways quite well reflect the behaviour of the trend of Nu numbers' characteristics. This means that the decisive parameter influencing such channels' thermal efficiency is the Nu number and not the friction factor f.

In the large Re number range, i.e., above 30,000, all channels calculated by method (a) have a PEC below unity. For the largest diameters of the inserts D = 0.8–0.9, the PEC is greater than one only for small numbers of Re in the range up to approx. 10,000. The highest PEC values are observed for inserts with diameters D = 0.5 and D = 0.4 with the smallest Re numbers. Therefore, it appears that the effective range of use for such inserts is the Re numbers less than 15,000.

According to the insert dimension, the thermal performance curves calculated by method (b) are arranged in a very regular way. The lowest PEC values are observed for the smallest insert diameter D = 0.2. With the increase of the insert diameter, the PEC increases regularly, and the highest values are reached for D = 0.9, with the maximum reaching over 8. As for a heat-flow channel with a single-phase flow, these are very high values. For this reason, one should approach these results and the associated method of calculating the Nu number with great care. Therefore, as mentioned before, the author recommends instead (a) calculating the Nu number based on the average gas temperature in the pipe's entire volume.

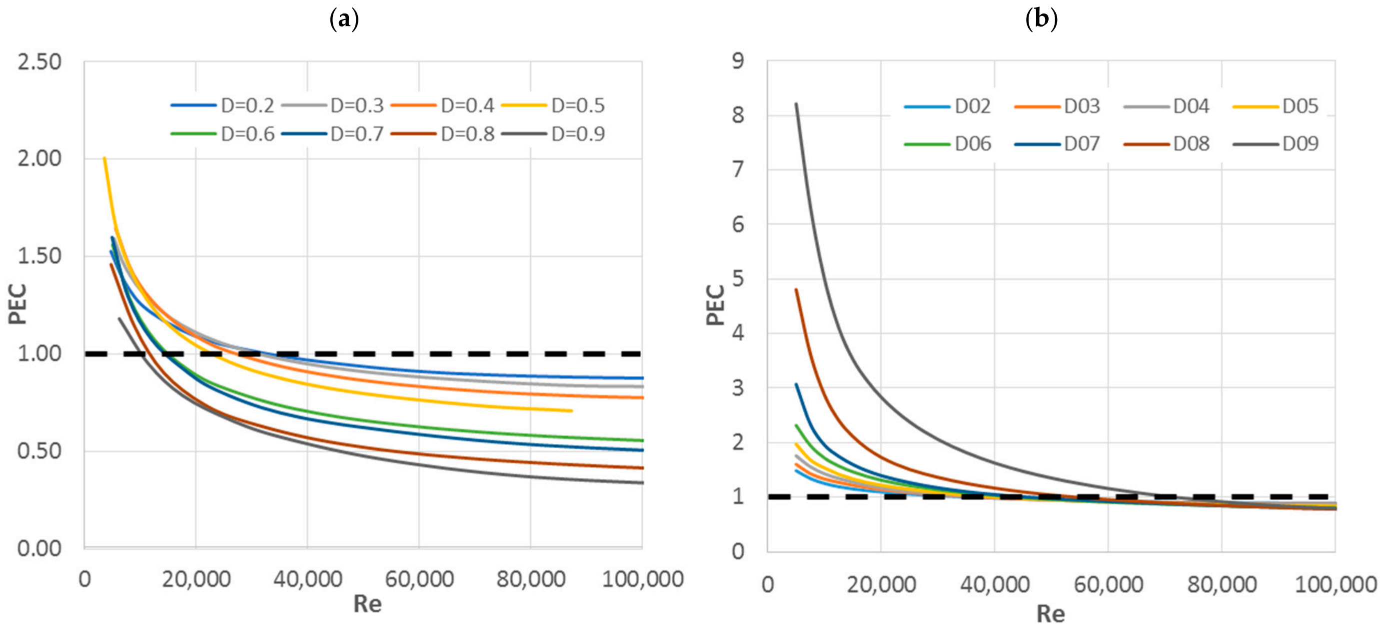

Figure 11. PEC(*Re*) characteristics calculated by two methods: (**a**) for the average temperature of the entire pipe section; (**b**) for the average temperature of the annular section.

Figure 12 shows the PEC characteristics for several Re numbers as a function of the dimensionless insert diameter D. For method (a), we can see the maxima of the function for diameters $D = 0.4$ and $D = 0.5$ at small Re numbers <10,000, while for Re numbers in the range 10,000–20,000 maximum shifts towards diameters $D = 0.3$ and $D = 0.4$. This means that for the smallest Re numbers, an insert with a diameter of $D = 0.5$ achieves the highest PEC, and with slightly larger Re numbers, up to about 20,000, an insert $D = 0.3$. With method (b), with increasing diameter D, the PEC characteristics trend is also upward, and the highest values are observed for the largest insert $D = 0.9$ and the smallest Re numbers.

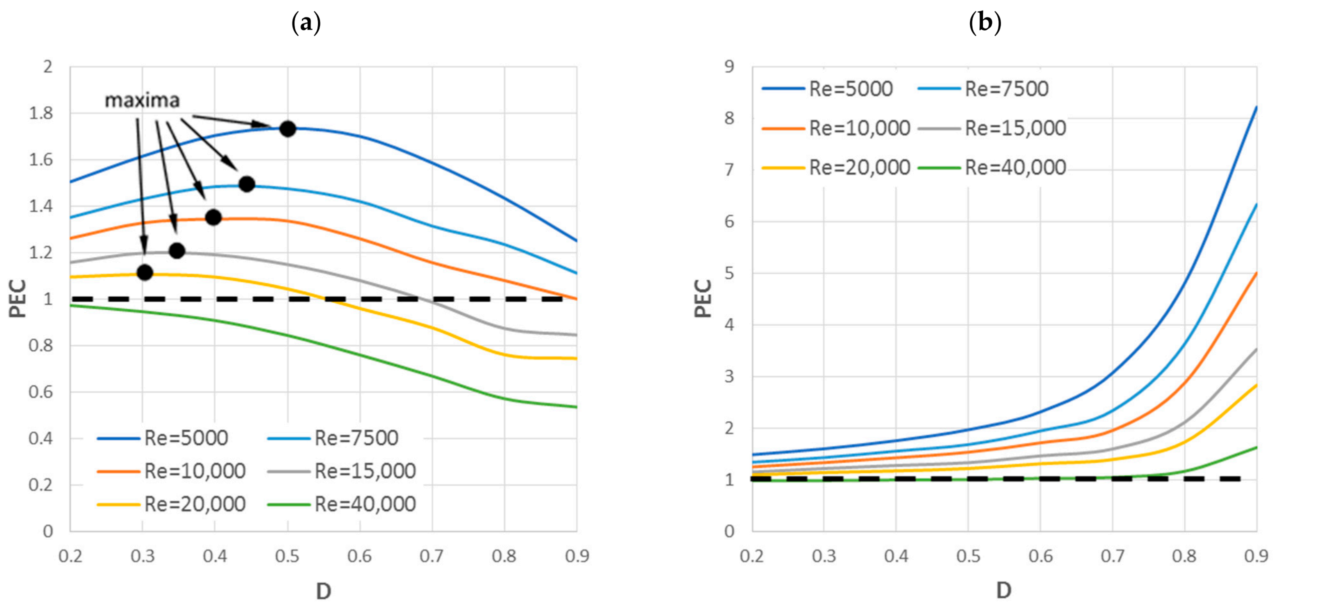

Figure 12. PEC(*D*) characteristics calculated by two methods: (**a**) for the average temperature of the entire pipe section; (**b**) for the average temperature of the annular section.

6. Summary and Conclusions

This work, which is Part 2 of the article, presents the results of numerical investigations for various sizes of heat transfer intensifying inserts, using the phenomenon of thermal radiation absorption. On the basis of the obtained results, heat flux balances were shown and described, and their characteristics were plotted. The diagrams in Figure 6 show the heat fluxes for the pipe wall, and Figure 7 illustrate the heat fluxes for the tested inserts. Figure 5 also shows the temperature insert characteristics as a function of the Re number, and Figure 8 shows the fields and temperature profiles in the pipe cross-section.

In order to calculate the thermal efficiency of the inserts, the relationships of the friction factor and Nu number in relation to a smooth pipe—$f/f_s(Re)$ and $Nu/Nu_s(Re)$ were presented. Based on the Formula (7), the PEC coefficient was calculated, and in Figure 11, its characteristics for the tested geometries are present—for the two described methods of calculating the Nu number.

The analysis of the results allowed for the formulation of the following conclusions:

(1) The highest insert temperatures are observed for small Re numbers, and they decrease with increasing Re numbers. As it is known from the Stefan–Boltzmann law for grey bodies (11), the greater the temperature difference among the surfaces, the greater the radiative heat flux transferred between them. In the case of the tested inserts, the magnitude of this flux is also influenced by the ratio of the heat transfer surfaces A_1/A_2, which is different in each geometry due to the changing insert diameter. According to Figure 5, the largest temperature differences ΔT and the greatest radiative heat fluxes are noted for the largest Re numbers.

(2) The fractions of these fluxes in relation to the total flux are shown in Figure 6. As can be seen, the largest radiative heat fluxes are absorbed by the inserts with the largest diameters, and the largest convective heat fluxes occur for the smallest insert's diameters. In general, for all studied inserts, as the Re number increases, the radiative heat flux decreases and the convective flux increases.

(3) The fractions of convective heat fluxes on both sides of the insert, in relation to the radiation flux absorbed by it, are shown in Figure 7. The presented graphs show negative values and values greater than 1. Negative fractions in Figure 7a mean that the convective heat flux has changed direction, and now the insert from the outer side is additionally heated by the flowing gas. Related to it is a convective heat flux directed to the inside of the insert, for which fractions greater than one were observed, Figure 7b. This notation means that thermal energy is transferred by convection from the insert's outer space to its interior. It can therefore be said that for such cases, the insert only acts one-sidedly, which generally significantly reduces the overall intensification of heat transfer. In Figure 8 can be seen that at high Re numbers, the gas's temperature in the annular cross-section is higher than the inserts, which causes its convection heating. With dimensionless diameters D = 0.8 and D = 0.9, two inserts work like this throughout almost the entire range of Re numbers.

(4) The thermal efficiency (PEC), depending on the calculation method, differs significantly from each other. As shown in Figure 11, the max PEC value calculated by method (a) is approx. 2 for the insert diameter D = 0.5, while the value calculated by method (b) reaches a value over 8 for D = 0.9. It can be noticed that the characteristics calculated by method (b) are arranged in a very orderly manner—their value increases with the insert diameter. The lowest PEC values are observed for the smallest insert diameter D = 0.2, and the highest values for D = 0.9, with the maximum reaching over 8.

Figure 12 shows the PEC characteristics for several Re numbers as a function of the dimensionless insert diameter D. Thus, for method (a), the maxima of the function are observed for diameters D = 0.4 and D = 0.5, and small Re numbers up to 10,000, while for Re numbers in the range 10,000–20,000 the maxima move towards the diameters D = 0.3 and D = 0.4. This means that an insert with a diameter of D = 0.5 has the highest PEC for the smallest Re numbers, while for slightly larger Re numbers reaching approx. 20,000, an insert with a diameter D = 0.3 has the highest PEC values. On the other hand, for manner (b), with increasing diameter D, the trend of the function on the graph is also upward, and the highest PEC values, as previously mentioned, are noticed for the largest insert D = 0.9.

Considering the criterion of thermal efficiency, the most optimal dimensions of the inserts are diameters D = 0.4 and D = 0.5, and for the range of small numbers, Re < 15,000.

(5) In numerical tests, the same emissivity of the pipe's inner surface and the insert equal to $\varepsilon = 0.9$ was used because these values better correspond to actual conditions. As it results from the Stefan–Boltzmann law and Equation (11), increasing the emissivity of such surfaces will increase the radiative heat flux and the thermal efficiency of such a tube.

The presented results were obtained for a relatively small temperature difference $\Delta T = 100\ ^\circ\mathrm{C}$, as for radiation processes. There is a need for further investigation of such inserts for larger temperature differences in order to determine their thermal efficiency and thermal-flow characteristics. Another interesting research issue is the consideration in calculations of the radiation properties of the working gases, i.e., water vapour and carbon dioxide, which are only partially permeable to radiation. This means that in addition to the convective heat transfer, these gases also heat up in their entire volume, absorbing part of the radiation.

It seems that the concept of such an insert may be of great importance, especially for high-temperature heat-flow processes, where radiation is the dominant method of heat transfer. Therefore, at large temperature differences, one can expect much higher thermal efficiencies of such channels.

Funding: This research received no external funding.

Institutional Review Board Statement: Not applicable.

Informed Consent Statement: Not applicable.

Data Availability Statement: Not applicable.

Conflicts of Interest: Author declare no conflict of interest.

Nomenclature

A	heat transfer area (m^2)
d_i	insert diameter (m)
d_p	pipe diameter (m)
D	diameter ratio, ($d_\mathrm{i}/d_\mathrm{p}$)
dp/dx	pressure gradient (Pa/m)
f	friction factor
k	thermal conductivity (W/mK)
L	domain length (m)
Nu	Nusselt number
$\dot{Q}_\mathrm{tot}$	total heat flux (W/m^2)
$\dot{Q}_\mathrm{rad}$	radiative heat flux (W/m^2)
$\dot{Q}_\mathrm{conv}$	convective heat flux (W/m^2)
PEC	Performance Evaluation Criteria
Pr	Prandtl number
Re	Reynolds number
T_b	bulk temperature (K)
T_w	wall temperature (K)
u	average velocity (m/s)
$\overline{U}$	vector of velocity (m/s)
v	kinematic viscosity (m^2/s)
ΔT	temperature difference (K)
ε	emissivity

ε_{12} interchange factor
ρ density (kg/m^3)
μ dynamic viscosity (Pa·m)
τ_w wall shear stress (Pa)
indexes:
s smooth tube
1 for smaller heat transfer area
2 for bigger heat transfer area

References

1. Bas, H.; Ozceyhan, V. Heat transfer enhancement in a tube with twisted tape inserts placed separately from the tube wall. *Exp. Therm. Fluid Sci.* **2012**, *41*, 51–58. [CrossRef]
2. Jasiński, P.B. Numerical study of thermal-hydraulic characteristics in a circular tube with ball turbulators. Part 3: Thermal performance analysis. *Int. J. Heat Mass Transf.* **2017**, *107*, 1138–1147. [CrossRef]
3. Bitama, W.; Demaghb, Y.; Hachicha, A.A.; Benmoussa, H.; Kabar, Y. Numerical investigation of a novel sinusoidal tube receiver for parabolic trough technology. *Appl. Energy* **2018**, *218*, 494–510. [CrossRef]
4. Ozceyhan, V.; Gunes, S.; Buyukalaca, O.; Altuntop, N. Heat transfer enhancement in a tube using circular cross sectional rings separated from wall. *Appl. Energy* **2008**, *85*, 988–1001. [CrossRef]
5. Tu, W.; Wang, Y.; Tang, Y. A numerical study on thermal-hydraulic characteristics of turbulent flow through a circular tube fitted with pipe inserts. *Appl. Therm. Eng.* **2016**, *101*, 413–421. [CrossRef]
6. Wang, W.; Zhang, Y.; Lee, K.-S.; Li, B. Optimal design of a double pipe heat exchanger based on the outward helically corrugated tube. *Int. J. Heat Mass Transf.* **2019**, *135*, 706–716. [CrossRef]
7. Zheng, Z.-J.; Li, M.; He, Y.-L. Thermal analysis of solar central receiver tube with porous inserts and non-uniform heat flux. *Appl. Energy* **2017**, *185*, 1152–1161. [CrossRef]
8. Alijani, M.R.; Hamidi, A.A. Convection and radiation heat transfer in a tube with core rod insert at high temperature. *Heat Mass Transf.* **2014**, *51*, 911–919. [CrossRef]
9. Alijani, M.R.; Hamidi, A.A. Convection and radiation heat transfer in a tube with core rod and honeycomb network inserts at high temperature. *J. Mech. Sci. Technol.* **2013**, *27*, 3487–3493. [CrossRef]
10. Zhang, J.; Sutton, W.; Lai, F. Enhancement of heat transfer using porous convection-to-radiation converter for laminar flow in a circular duct. *Int. J. Heat Mass Transf.* **1996**, *40*, 39–48. [CrossRef]
11. Jasiński, P.B. Numerical study of heat transfer intensification in a circular tube using a thin, radiation-absorbing insert. Part 1: Thermo-hydraulic characteristics. *Energies* **2021**, in press.
12. Gutkowski, A. Numerical Analysis of Flame Behavior Near the Quenching Conditions During Passage from Wider to Narrower Tube Diameters. *Combust. Sci. Technol.* **2012**, *184*, 1616–1634. [CrossRef]
13. Kacprzak, K.; Liskiewicz, G.; Sobczak, K. Numerical investigation of conventional and modified Savonius wind turbines. *Renew. Energy* **2013**, *60*, 578–585. [CrossRef]
14. Fodemski, T.; Górecki, G.; Jasiński, P. Corrugated channels heat transfer efficiency Analysis based on velocity fields resulting from computer simulation and PIV Measurements. In Proceedings of the 8th International Conference on Heat Transfer, Fluid Mechanics and Thermodynamics, HEFAT 2011, Pointe Aux Piments, Mauritius, 11–13 July 2011.
15. Kryłłowicz, W.; Magiera, R.; Łagodziński, J.; Sobczak, K.; Liskiewicz, G. Aerodynamical and structural design of the diagonal blower and its numerical and experimental validation. *J. Vib. Eng. Technol.* **2014**, *2*, 459–468.
16. Jasiński, P.B. Numerical study of thermal-hydraulic characteristics in a circular tube with ball turbulators. Part 1: PIV experiment and pressure drop. *Int. J. Heat Mass Transf.* **2014**, *74*, 48–59. [CrossRef]
17. Jasiński, P.B. Numerical study of thermal-hydraulic characteristics in a circular tube with ball turbulators. Part 2: Heat transfer. *Int. J. Heat Mass Transf.* **2014**, *74*, 473–483. [CrossRef]
18. Woźniak, D.; Obidowski, D.; Papierski, A. CFD based optimization of a semi-open impeller centrifugal pump for circulatory support. *Int. J. Artif. Organs* **2015**, *38*, 380.
19. Jasiński, P. Numerical Study of Friction Factor and Heat Transfer Characteristics for Single-Phase Turbulent Flow in Tubes with Helical Micro-Fins. *Arch. Mech. Eng.* **2012**, *59*, 469–485. [CrossRef]
20. Jasiński, P. Numerical optimization of flow-heat ducts with helical micro-fins, using Entropy Generation Minimization (EGM) method. In Proceedings of the WSEAS International Conferences (HTE'11), Florence, Italy, 23–25 August 2011; pp. 47–54.
21. ANSYS-CFX Manual v. 18.1. Available online: http://www.ansys.com (accessed on 25 July 2021).
22. Gutkowski, A.N.; Łęcki, M.; Jasiński, P.; Jędrowiak, B. Flame behavior during propagation in small isothermal tubes characterized by different degrees of the end opening. *Combust. Sci. Technol.* **2018**, *191*, 711–725. [CrossRef]
23. Zheng, N.; Liu, P.; Wang, X. Numerical simulation and optimization of heat transfer enhancement in a heat exchanger tube fitted with vortex rod inserts. *Appl. Therm. Eng.* **2017**, *123*, 471–484. [CrossRef]
24. Huanga, S.; Chena, H.; Zhang, X. Experimental evaluation of thermal performance in a circular tube with Y-branch insert. *Int. Commun. Heat Mass Transf.* **2019**, *106*, 15–21. [CrossRef]

25. Jasiński, P.; Kowalczyk, M.; Romaniak, A.; Warwas, B.; Obidowski, D.; Gutkowski, A. Investigation of Thermal-Flow Characteristics of Pipes with Helical Micro-Fins of Variable Height. *Energies* **2021**, *14*, 2048. [CrossRef]
26. Hasanpour, A.; Farhadi, M.; Sedighi, K. A review study on twisted tape inserts on turbulent flow heat exchangers: The overall enhancement ratio criteria. *Int. Commun. Heat Mass Transf.* **2014**, *55*, 53–62. [CrossRef]
27. Chang, C.; Sciacovelli, A.; Wu, Z.; Li, X.; Li, Y.; Zhao, M.; Deng, J.; Wang, Z.; Ding, Y. Enhanced heat transfer in a parabolic trough solar receiver by inserting rods and using molten salt as heat transfer fluid. *Appl. Energy* **2018**, *220*, 337–350. [CrossRef]
28. Liu, G.; Yang, C.; Zhang, J.; Zong, H.; Xu, B.; Qian, J.-Y. Internal Flow Analysis of a Heat Transfer Enhanced Tube with a Segmented Twisted Tape Insert. *Energies* **2020**, *13*, 207. [CrossRef]
29. Wijayanta, A.T.; Pranowo; Mirmanto; Kristiawan, B.; Aziz, M. Internal Flow in an Enhanced Tube Having Square-cut Twisted Tape Insert. *Energies* **2019**, *12*, 306. [CrossRef]
30. Bellos, E.; Tzivanidis, C. Enhancing the Performance of Evacuated and Non-Evacuated Parabolic Trough Collectors Using Twisted Tape Inserts, Perforated Plate Inserts and Internally Finned Absorber. *Energies* **2018**, *11*, 1129. [CrossRef]
31. Ho, C.; Liu, Y.-C.; Yang, T.-F.; Ghalambaz, M.; Yan, W.-M. Convective heat transfer of nano-encapsulated phase change material suspension in a divergent minichannel heatsink. *Int. J. Heat Mass Transf.* **2021**, *165*, 120717. [CrossRef]
32. Ho, C.; Liu, Y.-C.; Ghalambaz, M.; Yan, W.-M. Forced convection heat transfer of Nano-Encapsulated Phase Change Material (NEPCM) suspension in a mini-channel heatsink. *Int. J. Heat Mass Transf.* **2020**, *155*, 119858. [CrossRef]